FAR-ULTRAVIOLET STUDY OF THE ζ-OPHIUCHI H II REGION

Yeon-Ju Choi[1,2], Kyoung-Wook Min[1], and Kwang-Il Seon[3]

[1] Korea Advanced Institute of Science and Technology (KAIST), 373-1 Guseong-dong, Yuseong-gu, Daejeon 305-701, Korea; zmzm83@kaist.ac.kr
[2] Korea Aerospace Research Institute (KARI), 169-84 Gwahak-ro, Yuseong-gu, Daejeon, 305-806, Korea
[3] Korea Astronomy and Space Science Institute (KASI), 61-1 Hwaam-dong, Yuseong-gu, Daejeon 305-348, Korea

ABSTRACT

We report the results of our analysis of the H II region around ζ Oph based on far-ultraviolet (FUV) spectral imaging observations, together with data made in other wavelengths. We found that scattering by dust grains of the FUV photons, which originate mostly from ζ Oph, dominates the FUV emission in this region, while contributions from the two-photon effects and molecular hydrogen fluorescence are not negligible. Unlike the Hα image, which shows dark shadows of the molecular clouds on the extended diffuse background, the FUV continuum image is featureless with a smooth intensity that decreases outward from the center, which is attributed to multiple scattering of photons originating from a single star that smears out the shape of the scattering dust clouds. Molecular hydrogen fluorescence emission is enhanced at the boundary of the H II region, especially in LDN 204 at its closest region facing ζ Oph. The region has a high temperature of ∼1000 K as well as high atomic and molecular hydrogen content with $n_H = \sim10^{1.8}$ cm^{-3} and $N(H_2) = \sim10^{22}$ cm^{-2}, respectively. Photoionization and dust-scattering simulations are conducted with the effects of molecular clouds included, and the results are compared with the corresponding Hα and FUV observations. The results suggest that the molecular clouds reside close to the H II region in front of ζ Oph and that they may partially overlap with the H II region.

Key words: H II regions – ISM: individual objects (ζ Ophiuchi) – ultraviolet: ISM

1. INTRODUCTION

ζ Ophiuchi (HD 149757), a member of the Sco OB association, is a young massive star located at $(l, b) = (6°.28, 23°.58)$ at a distance of ∼140 pc from the Sun (Perryman et al. 1997). Its age is estimated to be ∼3 Myr (Tetzlaff et al. 2010) and its mass ∼20 $M_\odot$ (Villamariz & Herrero 2005). The star is classified as an O9.5 V type (Morgan et al. 1955) with an effective temperature in the range of 32,000 K < T < 33,000 K (Wood et al. 2005), and it is believed to be rotating rapidly with the projected rotational velocity of $v \sin i \sim 400$ km s^{-1} (Howarth & Smith 2001). It is also one of the fast moving stars. The proper motion of the star has been measured to be $\alpha = 13 \pm 1$ mas yr^{-1} and $\delta = 25.5 \pm 0.6$ mas yr^{-1} (Perryman et al. 1997), which results in a space velocity of 19.3 ± 0.4 km s^{-1} relative to the local standard of rest (LSR) for a distance of ∼140 pc (Wood et al. 2005). The heliocentric radial velocity of ζ Oph is -10.7 km s^{-1} (Lesh 1968), which is +3.3 km s^{-1} relative to the LSR in the radial direction (Draine 1986). Hence, ζ Oph may have moved from its birthplace during the past few million years and made a new ionized region around it (Tachihara et al. 2000; Wood et al. 2005). Furthermore, a bow shock, formed in front of the star in the direction of the proper motion probably as a result of the interaction of the stellar wind with the surrounding material, is seen in the [O III] emission (Gull & Sofia 1979) and the *Infrared Astronomical Satellite* (*IRAS*) 60 μm (Van Buren & McCray 1988) images. The angular separation of the bow shock from ζ Oph is estimated to be ∼5′ according to the 24 μm image made by the *Spitzer Space Telescope* (Gvaramadze et al. 2012).

The H II region Sh2-27 created by the ionizing radiation from ζ Oph was first discovered by Sharpless (1959). According to the Wisconsin Hα Mapper image (Haffner et al. 2003), the H II region appears to be more or less circular and extended to ∼6° from the star, corresponding to a radius of ∼15 pc at a distance of 140 pc. The density of the H II region was estimated to be ∼4.0 cm^{-3} (Sembach et al. 1994; Draine 1986) with an assumed temperature (T) of ∼7000 K. Wood

et al. (2005) discussed photoionization models that would reproduce the observed profiles of the Hα surface brightness and the [N II]/Hα line ratio of the H II region around ζ Oph. They obtained a mean density of ∼2 cm^{-3} and argued that the region is porous with clumpy materials, which occupy 50%–80% of the volume and are surrounded by a low-density smooth medium. Many interstellar absorption lines in the visual and ultraviolet wavelengths, embedded in the broad stellar spectrum of ζ Oph, have been studied in relation to the intervening neutral and ionized materials in the direction toward the star (Morton 1975; Howk & Savage 1999). For example, Sembach et al. (1994), using the far-ultraviolet (FUV) observations of the Goddard High Resolution Spectrograph abroad the *Hubble Space Telescope*, identified three types of highly ionized gas along the sightline toward ζ Oph, which may have originated from three different regions: the photoionized gas in the expanding H II region, the collisionally ionized gas from the bow shock of ζ Oph or from the local cloud complex, and another highly ionized gas that could be related to an optically thin shock produced by the stellar wind.

ζ Oph resides in a dust-rich region of the Galaxy where a variety of cloud complexes also exist (Lynds 1962). The dark features in the Hα map of the H II region coincide with the molecular clouds LDN 156 and LDN 204, indicating that these dark clouds, being located in front of the H II region, may block the Hα emission of the H II region (Tachihara et al. 2000). The clouds also seem to interact with the H II region as evidenced by the outward motion of the low-density gas away from ζ Oph relative to the dense cores (Tachihara et al. 2000). Dust-scattering properties of the Ophiuchus region were studied by Sujatha et al. (2005) using the archival *Voyager* data made in the FUV wavelengths. They found that the FUV intensity was correlated with the strength of the local interstellar radiation field but not with the 100 μm *IRAS* emission. This suggests that the FUV emission in this region originates from scattering of star lights by optically thin dust layers in front of the clouds, which is unlike the thermal infrared emission associated with the dense

molecular clouds. They adopted the Heyney–Greenstein model (Henyey & Greenstein 1941) for dust scattering and estimated the albedo a and the phase function asymmetry factor g to be $a = 0.40$ and $g = 0.55$, respectively, which are consistent with the theoretical predictions of Weingartner & Draine (2001).

While these previous studies significantly advanced our understanding of the physical environment around ζ Oph, there still remain various issues to be addressed and arguments to be confirmed. One of the issues is the distribution of the molecular clouds seen in this region, especially in the direction of sightlines. These clouds seem to be situated in front of the H II region since the dark regions in Hα intensity with peculiar shapes correlate well with the regions of high dust-extinction values. However, it is not clear where they are located relative to the H II region or the central star, although they may overlap with the H II region as argued by Tachihara et al. (2000). Absorption line studies of the stars with known distances may give some clues regarding this issue (Sembach et al. 1994; Liszt et al. 2009), but their application is quite limited for large diffuse objects with complex features such as the ζ Oph cloud complex. In this regard, we note that recent dust-scattering simulations based on FUV emission maps have shown excellent results regarding distance estimations of various targets (Jo et al. 2012; Lim et al. 2013; Choi et al. 2013).

We would like to apply the same Monte Carlo simulation technique to study the interaction of the FUV photons that originate from ζ Oph with the molecular clouds and thereby estimate the distance to these molecular clouds by comparing the simulation results with the FUV emission map available for this region. As mentioned above, a similar dust-scattering simulation study has been conducted previously by Sujatha et al. (2005) for a wide region including the ζ Oph cloud complex, but the *Voyager* observations, on which the simulations were based, were made only for a small number of positions and the spatial features of the ζ Oph cloud complex were not resolved well. Hence, the study focused on the scattering properties of the diffuse clouds that might exist in addition to the dense molecular clouds that were assumed to be at a fixed distance of 160 pc from the Sun. Here, with a more complete emission map taken in the FUV wavelengths, we would like to obtain a better picture of how the dense molecular clouds are distributed in this H II region. Following the Introduction, we describe the results of observations and simulations in Sections 2 and 3, respectively, and conclude with a summary in Section 4.

2. OBSERVATIONS

For this work, we analyzed the data set that was obtained from the Far-ultraviolet Imaging Spectrograph (FIMS) on board the Korean microsatellite *STSAT*-1 (Seon et al. 2004; Lee et al. 2004). FIMS is an instrument optimized for the observations of diffuse FUV emission with a large field of view ($7°.5 \times 4'.3$) and a moderate spectral resolution($\lambda/\Delta\lambda \sim 550$) for a wavelength band of 1330–1720 Å. More information on the instrument and the general data processing procedures can be found in Edelstein et al. (2006a, 2006b). The wavelength band of FIMS is similar to that of *Galaxy Evolution Explorer* (*GALEX*), but the ζ Oph region was not observed by *GALEX* as it intentionally avoided bright stars to protect its detectors.

We present in Figure 1 the FUV continuum image, in which the extended region of $14° \times 14°$ around ζ Oph is plotted, together with the Hα map obtained from the sky survey by Finkbeiner (2003). The FUV image was constructed from the FIMS data with a wavelength range of 1360–1660 Å using the
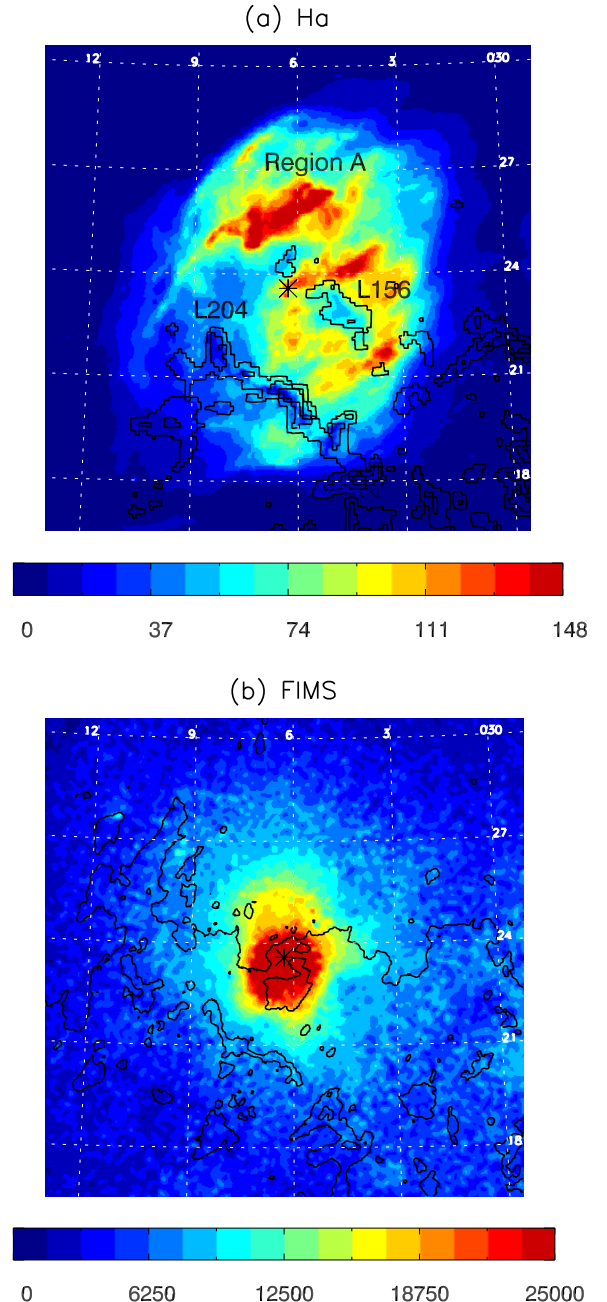

Figure 1. Hα image is overplotted with CO emission contours in panel (a) and the FUV image is overplotted with dust-extinction contours in panel (b). The images are shown in the Galactic coordinates and the central star ζ Oph is marked with an asterisk at $(l, b) = (6°.28, 23°.59)$.

HEALPix scheme (Górski et al. 2005) with a pixel resolution of $0°.1$. We removed the pixels of bright background stars based on the *TD-1* catalog (Thompson et al. 1978) and filled those deleted pixels by interpolating from neighboring pixels. The intensity level was saturated at 25,000 continuum units (photons sr^{-1} s^{-1} cm^{-2} Å^{-1}, henceforth CU) in this plot to suppress the dominating effect of the bright central star on the image. We also plotted the CO emission contours over the Hα map in Figure 1(a) and the dust-extinction contours over the FUV image in Figure 1(b). The CO contours are from the CO emission map of Dame et al. (2001), and the dust-extinction contours are based on the Galactic reddening map of the Schlegel, Finkbeiner, and Davis (SFD) Dust Survey (Schlegel et al. 1998).

Figure 1(a) shows dark regions coincident with the molecular clouds LDN 156 and LDN 204 on the bright Hα background of the H II region, which is confined to the inside of the angular radius of 6°. LDN 204 affects a broad region of the southeastern corner of the Hα map whereas the regions affected by LDN 156 seem to be well confined and bounded by bright regions. The decrease in the Hα intensity in the regions of the two clouds LDN 156 and LDN 204 from their surroundings accords well with the increase in the dust-extinction level. For example, the Hα intensity of ∼70 R at the center of LDN 156 is ∼25% lower than those of its immediate neighborhoods, which can be attributed to the increase of ∼0.1 in $E(B - V)$, the dust-extinction level. We also note that, while the Hα intensities are significantly low in the regions of the two clouds compared to their surroundings, they are still much brighter than those of the background outside the H II region: the Hα intensities in the middle of the two clouds are ∼70 R and ∼45 R for LDN 156 and LDN 204, respectively, whereas the background Hα intensity is ∼5 R. In view of high dust-extinction levels in these cloud regions, which are $E(B - V) = $ ∼0.6 for LDN 156 and $E(B - V) = $ ∼0.85 for LDN 204 and significantly higher than the background level of $E(B - V) = $ ∼0.2, the relatively high Hα intensity of these regions may indicate that at least part of the clouds are located inside the H II region so that a portion of the observed Hα emission does not suffer extinction by the clouds. The conspicuous bright feature above the central star, marked as Region A in Figure 1(a), seems to be the result of the hot and clumpy gas distribution, as it is also seen to be enhanced in dust temperature according to Figure 2 of Plank Collaboration (2011). The dust-extinction level of Region A is not much different from that of its neighborhood.

FUV emission is also prominent in the H II region around ζ Oph, as shown in Figure 1(b). In fact, this H II region is the second brightest diffuse object in FUV in the high Galactic latitude region following Sco-Cen and is brighter than the Spica nebula. When compared with Figure 1(a), the FUV intensity map is remarkably different from the Hα map. The FUV map exhibits a generally smooth profile, with a gradual decrease in its intensity outward from the center, which is in contrast to the Hα image that has prominent irregular features of bright and dark regions. We believe such a featureless image of the FUV map supports scattering as the origin of the FUV emission in this region. While dust scattering is predominant in the forward direction, the non-directional nature of scattering produces a smeared image, which is even intensified when the photons originate from a single star and when multiple scattering occurs. This is in sharp contrast to the Hα image with prominent features in which the foreground clouds produce clear shadows on the extended diffuse background of the Hα emission. We also note that while the dominant contribution to FUV intensity comes from dust scattering of stellar photons, a certain portion of the FUV continuum intensity is attributed to the two-photon continuum emission in the warm ionized medium, such as the object of this study. Hence, the two-photon effect should be subtracted from the observed FUV intensity to assess the true effect of dust scattering. Assuming a correspondence of 60 CU of FUV intensity to 1 rayleigh (R) of Hα (Reynolds 1990), based on the Hα map of Figure 1(a), we estimate the reduction of FUV intensity to be ∼5000 CU in the central core region.

As dust scattering is the dominant source of the diffuse FUV emission in this region, we have plotted in Figure 2 a pixel-to-pixel correlation plot for the FUV intensity against dust extinction for the region of 14° × 14° shown in Figure 1. The

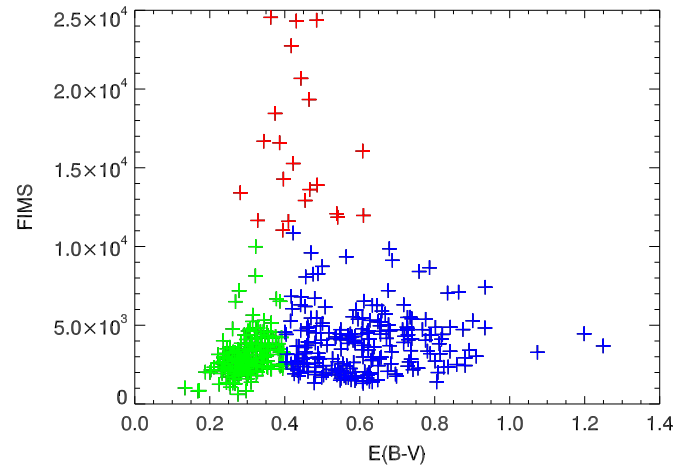**Figure 2.** Pixel-to-pixel scatter plot of FUV intensity against dust extinction for the entire 14° × 14° region shown in Figure 1.

red data points represent the central region inside the angular radius of 2° where the FUV intensity is higher than 10^4 CU, and the green and the blue data points are the area outside the central region, where the FUV intensity is less than 10^4 CU, with the $E(B - V)$ values smaller than 0.4 and larger than 0.4, respectively. Most of the green data points reside in the northern part above the central region whereas most of the blue data points reside in the southern part below the central region. The two-photon effect was removed in the FUV intensities shown in Figure 2. First, we see that the red data points, as their intensities are determined more or less by the distance from the star, are scattered and do not show any relation with $E(B - V)$. On the other hand, FUV intensity correlates with $E(B - V)$ in the northern region, as represented by the green data points, while it has a more or less flat distribution in the southern region, as represented by the blue data points. The southern region is optically thick and thus, the effects of foreground scattering and extinction, together with non-uniform interstellar radiation fields as a photon source for scattering, would yield the FUV intensity to fluctuate with no specific dependence on the dust-extinction levels. However, the positive correlation between the FUV intensity and $E(B - V)$ in the northern region seems interesting because the $E(B - V)$ values of the northern region, which are in the range of 0.2–0.4 and, though smaller than those of the southern region, are still large enough for the whole northern region to be regarded as optically thick in the FUV wavelength band since the $E(B - V)$ value of ∼0.14 corresponds to the optical depth of $\tau \sim 1$ at 1565 Å with the conversion factor $R_V = 3.1$. In view of the argument that the correlation between the FUV intensity and $E(B - V)$ holds in optically thin regions (Hurwitz 1994), the above observation may imply that a portion of the dust seen in the map actually resides behind the star so that the remaining dust in front of the star becomes optically thin in the FUV wavelengths. In this regard, we note that the $E(B - V)$ values in Figure 2 are generally above 0.2, which may be consistent with the idea that a more or less uniform background of $E(B - V) = $ ∼0.2 exists across the whole region of 14° × 14° shown in Figure 1.

Figure 3 presents the FUV spectra of ζ Oph and the surrounding region for the wavelength band of 1370–1670 Å. The top panel shows the spectrum of ζ Oph observed by the *International Ultraviolet Explorer* (*IUE*), and the middle and the bottom panels are the spectra observed by FIMS for the
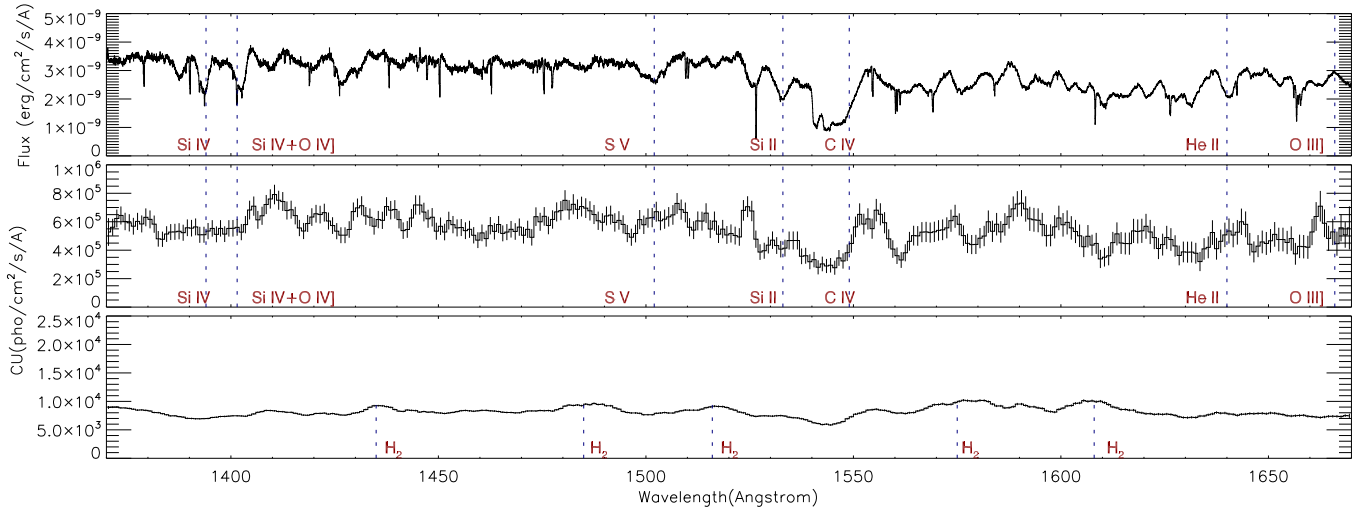
Figure 3. FUV spectrum of ζ Oph and the surrounding region: (a) *IUE* spectrum of ζ Oph, (b) FIMS spectrum observed for the region inside 0°.5 around ζ Oph, and (c) FIMS spectrum for the whole region of $14° \times 14°$ shown in Figure 1(a), with the central core region inside 0°.5 around ζ Oph removed from the plot.

core region within the angular radius of 0°.5 around the central star and the whole region of $14° \times 14°$ shown in Figure 1 except the core region with an angular radius of 0°.5 around ζ Oph, respectively. The short-wave prime *IUE* data (1150–2000 Å) were obtained with a spectral resolution of 0.04 Å from the Mikulski Archive for Space Telescopes at the Web site http://archive.stsci.edu/iue/. The FIMS spectrum of the central core region around ζ Oph in the middle panel, which was smoothed with a running average of three bins from the original 1 Å bins, corresponds well with the *IUE* spectrum, though some of the absorption line features are not as clear as those of the *IUE* spectrum because of smoothing and statistical fluctuations. In particular, the P Cygni profile of C IV at 1548 Å is also prominent in the FIMS spectrum of the core region. The spectrum of the bottom panel of Figure 3, obtained for the whole region of $14° \times 14°$ outside the central core region, still hints of the P Cygni profile of C IV as a broad feature, probably due to dust scattering of the photons that originate from the central core region. Furthermore, we note that the spectrum reveals molecular hydrogen fluorescence features, as indicated by the vertical dashed lines in panel (c).

Hence, we have plotted in Figure 4 the map of H_2 fluorescence emission intensity obtained from the emission line at 1608 Å, with CO contours overplotted on the same map. The pixel resolution is ∼1° in this figure, coarse-grained compared to the map of Figure 1(b) to improve the signal-to-noise ratio. It is seen that H_2 fluorescence emission is generally enhanced at the boundary of the H II region, which is reasonable because the region represents the interface between the ionized and the neutral media. The brightest H_2 fluorescence emission occurs in LDN 204, especially in the region closest to the central star. While Tachihara et al. (2000) suggested the inter-cloud regions, where CO molecules were not detected, to be candidate photodissociation regions (PDRs), the present low resolution images cannot discriminate the PDRs from the regions of molecular clouds.

3. MODELING AND DISCUSSIONS

3.1. Photoionization Simulation

We mentioned that relative changes in the Hα intensity from their surroundings for the regions of the molecular clouds LDN
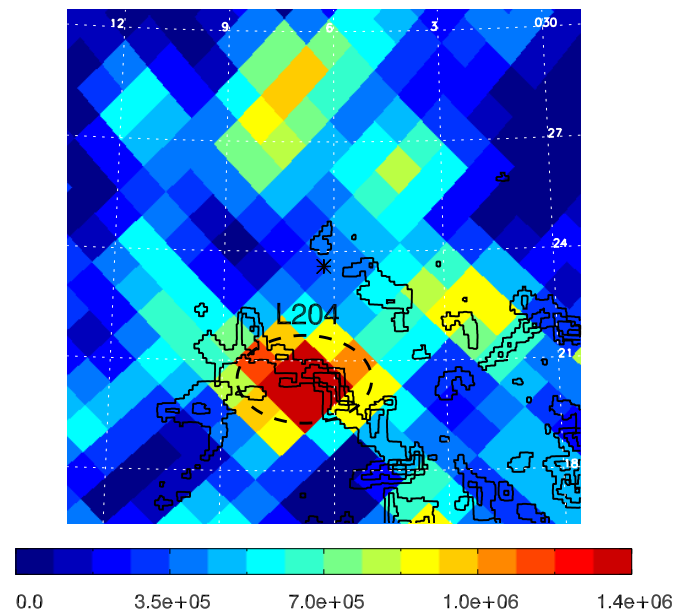

Figure 4. H_2 fluorescent emission map with the CO contour (in LU) of the ζ Oph region. The central star ζ Oph is marked with an asterisk at $(l, b) =$ (6°.28, 23°.59). The bright region of LDN 204, indicated by the dotted circle, will be modeled as a PDR in Section 3.

156 and LDN 204 are consistent with changes in the dust-extinction level, whereas the Hα intensities in these regions are still significantly higher than those of the background. Here, we describe our simulation of the Hα intensities for the H II region, using the photoionization model coupled with dust extinction, and compare the results with the observed intensities. We employ the photoionization code, the MOnte CArlo SimulationS of Ionized Nebulae (Ercolano et al. 2008), to establish the radial profile of a bare Hα intensity assuming spherical symmetry, using the parameters suggested by Wood et al. (2005). The stellar atmospheric model of Castelli & Kurucz (2004) is adopted for the central star, with the Lyman continuum luminosity Q(H) of 0.8×10^{47} photons s^{-1} and the temperature of 32,000 K in view of the stellar type O9.5 V of ζ Oph. The background density is set to be constant with 2 cm^{-3}. The abundance ratios of He, C, N, O, and S are set to be 0.1, 140, 75, 319, and 18 parts per
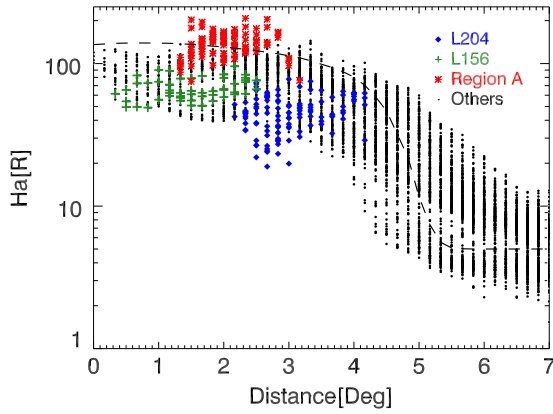
Figure 5. Hα intensities displayed against the angular distance from the central star. The data points corresponding to the bright Region A are shown in red, those corresponding to the molecular clouds LDN 156 and LDN 204 are shown in green and blue, respectively, and those corresponding to other pixels are shown in black. The dashed line is the simulated bare Hα profile (see the text).

million (ppm) relative to H (Sembach et al. 1994). We added the background of 5 R to the simulated radial profile of the bare Hα intensity.

The simulation result is shown as a dashed line in Figure 5, in which the Hα intensity drops sharply between $4°$ and $5°$, indicating the boundary of the H II region. The simulated result can be compared with the observations as the observed Hα intensities at pixel positions are also plotted as functions of the corresponding angular distance from the central star. We indicated the regions that correspond to the peculiar features shown in Figure 1(a). The data points corresponding to the bright Region A are shown in red; those corresponding to the molecular clouds LDN 156 and LDN 204 are shown in green and blue, respectively; and those corresponding to other pixels are shown in black. The observed data points are rather severely scattered, as can be expected from Figure 1(a), which may be caused by the irregular densities of the H II region as well as non-uniform dust distribution. We note that Wood et al. (2005) argued that the region is porous with a clumpy density distribution. Nevertheless, it is seen that most of the data points are below the simulated Hα profile except the red data points corresponding to the bright Region A, which is reasonable because dust extinction is not taken into account in the model. Region A could be a region of higher density and/or temperature than those assumed for the simulation.

Now, we apply dust extinction to the simulated bare Hα profile for each pixel and compare the result with the observed Hα map. We calculate the optical depth at 6563 Å for each pixel from the corresponding $E(B - V)$ value by multiplying the factor of 2.69. We assume a uniform background of $E(B - V) = 0.2$, which is subtracted from the observed dust-extinction values and a factor of $f(<1.0)$ is multiplied to the remaining value to accommodate the situation in which all of the remaining dust may not be in front of the H II region but a portion of it could be embedded in or located behind the H II region. Figure 6 shows the result with $f = 0.8$ for the region with an angular radius smaller than $5°$: (a) the difference between the observed and the simulated Hα maps and (b) the pixel-to-pixel scatter plot of the observed and simulated Hα intensities. While we made a number of assumptions for the simulation model, the result agrees with the observation reasonably, especially for the cloud regions of LDN 156 and LDN 204, which appear to be green or yellow in Figure 6(a), indicating that the simulated
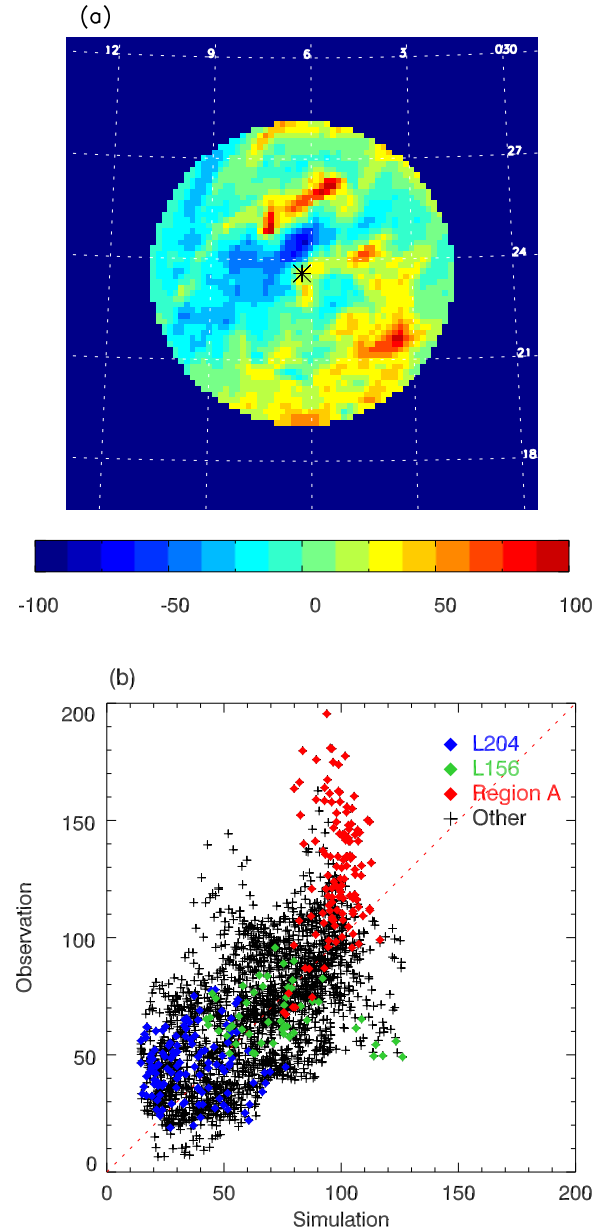

Figure 6. (a) Difference of the observed Hα map from the simulated Hα map and (b) the pixel-to-pixel scatter plot of the observed and simulated Hα intensities.

intensities of these regions are similar to those of observations. On the other hand, the region around LDN 156 and Region A are red, which indicates that the simulated intensities are significantly lower than the observed ones. The region right above the star is blue, indicating that the simulated intensity is higher than the observed intensity. These fluctuation imply that the densities and temperatures of the H II region are quite irregular. At the boundary of the H II region, the simulated intensity is generally lower than the observed intensity, which is caused by the H II region of the simulation model being smaller than the observation.

3.2. Dust-scattering Simulation

Now, let us turn to the FUV map of Figure 1(b) and show that the FUV emission seen in the H II region comes mostly from dust scattering. We adopt a three-dimensional Monte Carlo radiative transfer code developed previously and used successfully for

several targets (Seon & Witt 2012; Jo et al. 2012; Lim et al. 2013; Choi et al. 2013). The code allows multiple scattering and each scattering is represented by the Henyey–Greenstein function with adjustable parameters of albedo and the phase function asymmetry factor (Henyey & Greenstein 1941). In previous applications of the code, the albedo a, the asymmetry factor g, and the distance d and the thickness t of simplified model layers of dust are free parameters to be determined. However, in a situation in which a single star dominates the scattering effect such as in our study, these parameters are not uniquely determined and degenerate sets that give the same simulated image are possible. Hence, we fix a and g with reasonable values of $a = 0.4$, $g = 0.45$ in this study in view of the results of previous studies with FIMS data, which were in the range of 0.38–0.43 and 0.45–0.47, respectively (Jo et al. 2012; Lim et al. 2013; Choi et al. 2013), and allow only d and t to vary as free parameters. A similar study conducted by Sujatha et al. (2005) that covered a broad region including ζ Oph yielded $a = 0.40 \pm 0.10$ and $g = 0.55 \pm 0.25$ for 1100 Å of the *Voyager* observations. The theoretical predictions of a and g are in the range of 0.4–0.6 and 0.55–0.65 (Weingartner & Draine 2001), respectively. The value of g in the simulations with the FIMS data is a bit smaller than the theoretical estimation, probably because of smoothing of the data. To compare the dust-scattering simulation with the observation, the effects other than dust scattering that contribute to FUV emission should be subtracted from the observed FUV map. Hence, the two-photon effect is subtracted assuming 60 CU of FUV intensity per 1 R of Hα intensity, which is a reasonable assumption for H II regions (Reynolds 1990). However, as these FUV photons from the two-photon effects are also scattered by dust, it may not be correct if 60 CU is multiplied to the Hα intensity for each pixel and the result subtracted from the observed FUV intensity of the corresponding pixel. Instead, we simply take a mean value of 16% of the total FUV intensity to be of a two-photon effect origin, in view of the albedo of 0.4, and subtract 16% of the observed FUV intensity for each pixel over the whole region. Furthermore, as Figure 4 indicates, the fluorescent emission from molecular hydrogen may contribute significantly in the H II region boundary, especially in the bright H$_2$ emission region of LDN 204. This fluorescence emission is also subtracted from Figure 1(b) before the simulated map is compared with the observed image.

The simulation domain consists of $400 \times 400 \times 400$ rectangular grids with a grid size of 1 pc. The central axis is chosen along the line of sight toward ζ Oph, and the Sun is placed at the center of the front face of the simulation box. A total of 1499 stars based on the *TD-1* and *Hipparcos* catalogs are distributed in the simulation box as radiation sources. A total number of 10^8 photons are generated and assigned to stars according to their intrinsic luminosities. The SFD dust survey map (Schlegel et al. 1998) is used for the spatial distribution of dust. However, as the map provides only the two-dimensional information projected onto the sky with integrated $E(B - V)$, we need to distribute the observed extinction along the sight lines. We simplify the model by assuming that the clouds consist of a few slabs. Hence, the result of the present simulation should be regarded as an idealized model with equivalent dust distribution, not a unique and accurate model. To constrain the parameter space further, we use the following results of observations. According to Liszt et al. (2009), the extinction value of ζ Oph is 0.32, whereas the $E(B - V)$ value close to ζ Oph is 0.55 according to the SFD map in Figure 2, implying that the remaining $E(B - V) = 0.23$ is behind the star. Furthermore, Sembach et al. (1994)

and Liszt et al. (2009) argued that a small cloud of $N(\text{H I}) = 5.2 \times 10^{20}$ cm^{-2} and $N(\text{H}_2) = 4.5 \times 10^{20}$ cm^{-2}, corresponding to $E(B - V) = 0.25$ with a ratio of $N(\text{H I})$ to $E(B - V)$ taken to be 5.8×10^{21} cm^{-2}, exists in front of and close to the star. In view of these observations, we assume a distribution of dust that consists of four components: a background of $E(B - V) = 0.2$, which is subtracted from the observed SFD values, a small cloud placed in front of the star with both a diameter and a thickness of 2 pc, a uniform thin dust medium that surrounds ζ Oph, and a dense cloud component. The thicknesses of and the distances to the thin dust medium as well as the dense cloud are free parameters to be determined. The extinction values corresponding to the small cloud in front of the star, the thin uniform dust medium, and the dense cloud component are also determined by comparing the simulated image with the observed map. Since there are many parameters to be determined, hundreds of simulations were carried out to find the best set of parameters. The final set of parameters we obtained is as follows: 0.22 for the extinction value of the small cloud in front of ζ Oph; the thickness of the thin uniform dust medium is 25 pc, spanning from 125 pc to 150 pc, with $E(B - V)$ given by the SFD value subtracted by the background value of 0.2, bounded by the maximum value of 0.4; and the remaining dust located between 130 and 135 pc corresponding to the dense clouds. While these chosen values may not be the unique and best set of parameters even for the current idealized four-slab model, the result seen in Figure 7 is quite impressive, which indicates that the present simple model may resemble the realistic distribution in certain aspects which must consist of clumpy and irregular dust clouds. In this regard, we note the location of the dense cloud component, which overlaps the H II region partially in front of the star. The current result is in agreement with Tachihara et al. (2000), in which it was argued that the clouds interact with the H II region.

3.3. PDR Simulation

In this section, we model the H$_2$ fluorescence emission seen in Figure 4 as a PDR candidate. In PDRs, H$_2$ molecules are dissociated when they absorb FUV photons of the Lyman and Werner bands in $\sim$10% of the cases. In the remaining $\sim$90% of the cases, the H$_2$ molecules are de-excited, on a timescale of 10^{-8} s, to the vibrationally excited states of the ground electronic level by emitting FUV emission lines. We focus here on the circled region of LDN 204 in Figure 4, whose spectrum is shown in Figure 8 with clear H$_2$ fluorescence emission features. We adopt the simulation code CLOUD (van Dishoeck & Black 1986), a plane-parallel H$_2$ model program, to constrain the physical quantities of this region. The simulation takes the following free parameters that are to be determined by comparing the simulated results with the observations: n_H (hydrogen density), T (cloud temperature), $N(\text{H}_2)$ (molecular hydrogen column density), and I_UV (external FUV radiation fields). Among these parameters, we fix the value of I_UV assuming ζ Oph is the only radiation source for LDN 204. With the integrated luminosity of the star of 7.2×10^{45} photons s^{-1} over the wavelength 912 Å $< \lambda <$ 1130 Å, the external FUV radiation field becomes $I_\text{UV} = \sim 1$ assuming the distance between ζ Oph and the region of interest in LDN 204 to be $\sim$5 pc. The ranges of parameters were chosen as follows : 10^1–10^4 K for the temperature T, $10^{1.5}$–10^3 cm^{-3} for the hydrogen density, n_H, 10^{20}–$10^{22.3}$ cm^{-2} for the molecular hydrogen column density $N(\text{H}_2)$. The best-fit
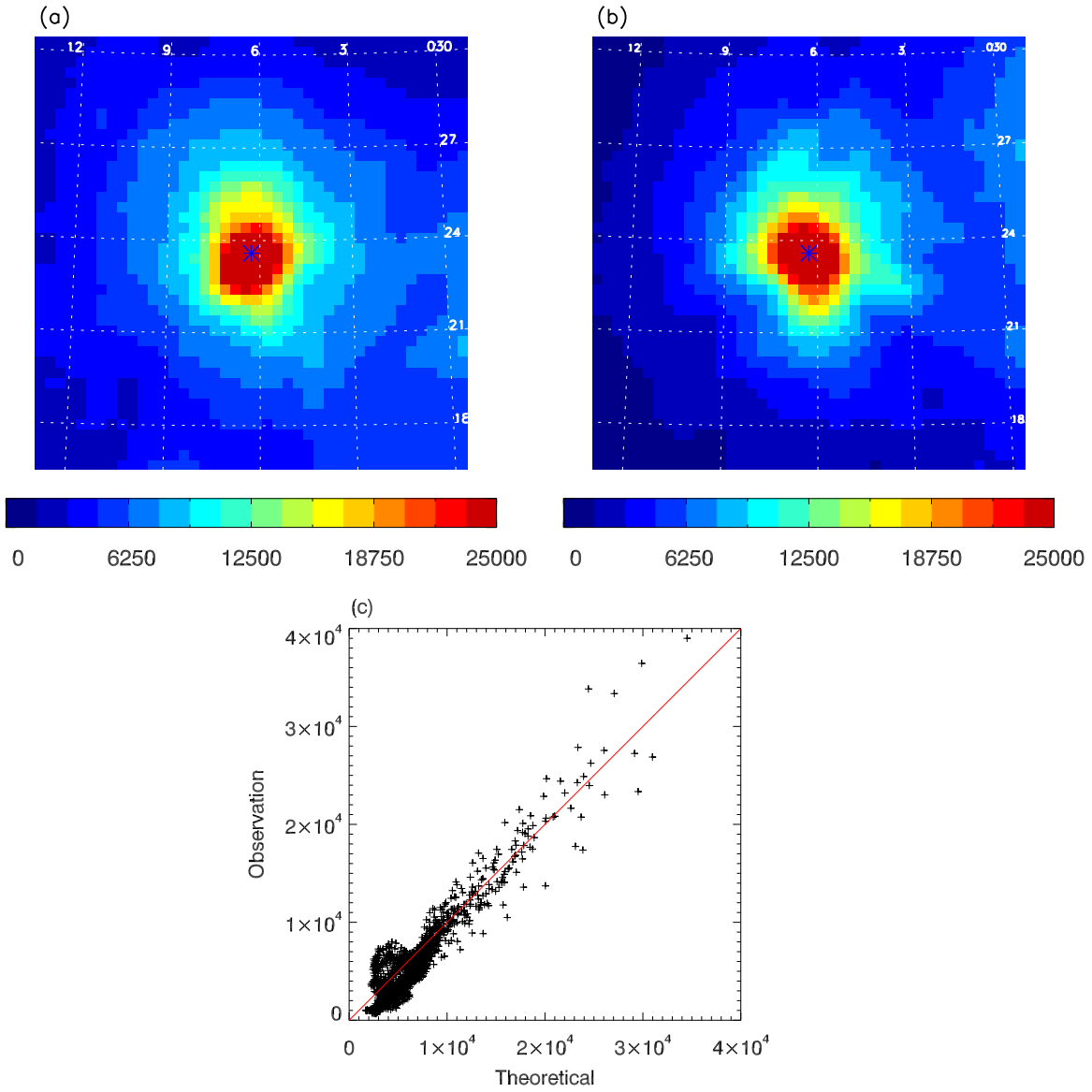
Figure 7. FUV continuum map of the simulated (a) and the observed (b) FUV intensities; see the text for the parameters corresponding to panel (a). A pixel-to-pixel correlation plot of the FUV intensities of panels (a) and (b) is shown in panel (c).
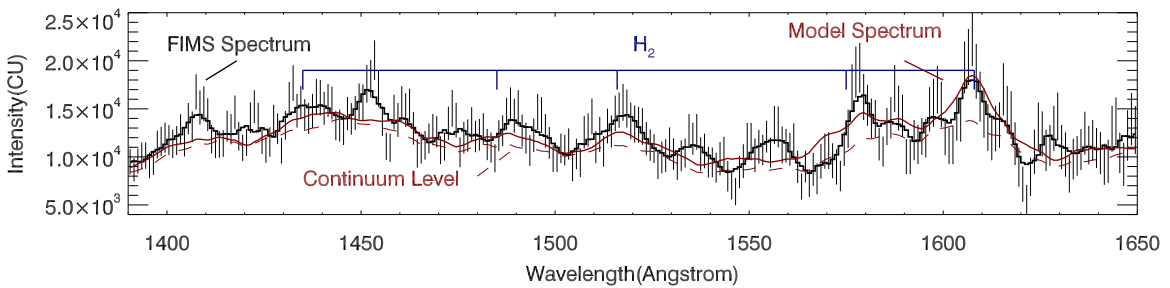

Figure 8. FUV spectrum obtained from the circled region of LDN 204 in Figure 4, and the best-fit result of the PDR model, depicted as a solid line. The continuum level is determined from the interpolation of the minimum data points and represented as a dashed red line.

result is $T = 1000$ K, $n_H = 10^{1.8}$ cm^{-3}, and $N(H_2) = 10^{22}$ cm^{-2}, and the corresponding spectrum is shown as a red solid line in Figure 8. The high temperature of 1000 K has been seen in a simulation for PDR regions (Ryu et al. 2006; Jo et al. 2011). It is remarkable that Tachihara et al. (2000) also estimated the molecular hydrogen column density to be $\sim 1.1 \times 10^{22}$ cm^{-2} for the same region based on the radio observation of C^{18}O.

3.4. Discussions

First, let us summarize what we have learned from the observations and simulations as described in the previous sections. Of the observed $E(B - V)$ in this region, a small portion, $E(B - V) \sim 0.2$, seemed to be located behind the H II region, as implied by the SFD map and the scatter plot

of FUV intensity against dust extinction shown in Figure 2. The remaining $E(B - V)$ values in the regions of LDN 156 and LDN 204 were still too high to account for the observed Hα intensities in these regions, and it was suspected that a certain amount of the Hα emission from the H II region escapes without suffering from extinction: according to the photoionization simulations, $\sim$80% of the remaining extinction values were required to reproduce the observed intensities. The simulations also revealed that the densities and temperatures of the H II region are quite irregular. The result of dust-scattering simulations based on the FUV emission map indicated that the molecular clouds overlap with the foreground H II region. These molecular clouds seemed to be embedded in a diffuse dust component that is pervasive throughout the region.

These observations and simulations indicate that the molecular clouds in this region are close to and overlap with the H II region, which is consistent with the observation by Tachihara et al. (2000) that the clouds interact with the H II region. Wood et al. (2005), based on the studies of line ratio of [N II] to Hα intensities, argued that the majority of the gas in the H II region is distributed in clumps in a smooth low-density component. While the present study focused only on the dust clouds and the simulation did not model clumpy dust distribution, the result, that the dust associated with the clouds does not fully participate in extinction, is not inconsistent with the clumpy distribution of dust since the Hα photons from the H II region can pass through the clouds more easily with less extinction between the clumps.

The present observation showed enhanced molecular hydrogen fluorescence emission at the boundary of the H II region, with a peak intensity seen in the region of LDN 204 facing the central star. The PDR simulation predicted the column density of molecular hydrogen in the LDN 204 region to be $N(\text{H}_2) = 10^{22}$ cm^{-2} at a temperature of $T = 1000$ K, in agreement with the result based on radio observations (Tachihara et al. 2000). Draine (1986) constructed a multi-fluid shock model consistent with the observed molecular lines toward ζ Oph, and argued that a large fraction of high rotational states of molecular hydrogen seen along the sightline should come from the shock transition layer. However, the portion of molecular hydrogen within the shock layer takes up only $\sim$1% ($\sim$5 $\times$ 10^{18} cm^{-2}) of the total column density observed toward ζ Oph, which is much less than the column density for the LDN 204 region. Hence, we believe the contribution from the shock proposed by Draine (1986) has a negligible contribution to the molecular hydrogen fluorescence emissions depicted in Figure 4. Furthermore, the proposed shock speed of 9 km s^{-1} is too slow to produce emission lines from highly ionized species that can be observed in FUV wavelengths.

4. SUMMARY

We analyzed the data sets of the FUV observations performed by FIMS, together with the maps constructed in other wavelengths, for the ζ Oph H II regions, including the prominent molecular clouds. We confirmed that the FUV emission seen in this region is mostly due to dust scattering of the photons originating from the central star ζ Oph, while contributions from the two-photon effect and the molecular hydrogen fluorescence are not negligible. The photoionization model showed that the Hα

emission from the H II region does not suffer from dust as much as expected from the color excess values, implying that dust clouds may partially overlap with the H II region while a clumpy distribution of dust may not be ruled out. Dust-scattering simulations of FUV photons from ζ Oph as well as nearby stars also indicated overlapping of dust clouds with the H II region, with the entire clouds complex embedded in a pervasive distribution of diffuse dust. Molecular hydrogen fluorescence emission is seen at the boundary of the H II region with peak enhancement in the region of LDN 204, which is well modeled as a PDR.

REFERENCES

Castelli, F., & Kurucz, R. L. 2004, arXiv:astro-ph/0405087
Choi, Y.-J., Min, K.-W., Seon, K.-I., et al. 2013, ApJ, 774, 34
Dame, T. M., Hartmann, D., & Thaddeus, P. 2001, ApJ, 547, 792
Draine, B. T. 1986, ApJ, 310, 408
Edelstein, J., Korpela, E. J., Adolfo, J., et al. 2006a, ApJL, 644, L159
Edelstein, J., Min, K.-W., Han, W., et al. 2006b, ApJL, 644, L153
Ercolano, B., Young, P. R., Drake, J. J., et al. 2008, ApJS, 175, 534
Finkbeiner, D. P. 2003, ApJS, 146, 407
Górski, K. M., Hivon, E., Banday, A. J., et al. 2005, ApJ, 622, 759
Gull, T. R., & Sofia, S. 1979, ApJ, 230, 782
Gvaramadze, V. V., Langer, N., & Mackey, J. 2012, MNRAS, 427, L50
Haffner, L. M., Reynolds, R. J., Tufte, S. L., et al. 2003, ApJS, 149, 405
Henyey, L. G., & Greenstein, J. L. 1941, ApJ, 93, 70
Howarth, I. D., & Smith, K. C. 2001, MNRAS, 327, 353
Howk, J. C., & Savage, B. D. 1999, AJ, 117, 2077
Hurwitz, M. 1994, ApJ, 433, 149
Jo, Y.-S., Min, K.-W., Lim, T.-H., Seon, K.-I., et al. 2012, ApJ, 756, 38
Jo, Y.-S., Min, K.-W., Seon, K.-I., et al. 2011, ApJ, 738, 91
Lee, D.-H., Seon, K.-I., Park, J.-H., et al. 2004, JASS, 21, 391
Lesh, J. R. 1968, ApJS, 17, 371
Lim, T.-H., Min, K.-W., & Seon, K.-I. 2013, ApJ, 765, 107
Liszt, H. S., Pety, J., & Tachihara, K. 2009, A&A, 499, 503
Lynds, B. T. 1962, ApJS, 7, 1
Morgan, W. W., Code, A. D., & Whitfort, A. E. 1955, ApJS, 2, 41
Morton, D. C. 1975, ApJ, 197, 85
Perryman, M. A. C., Lindegren, L., Kovalevsky, J., et al. 1997, A&A, 323, L49
Plank Collaboratoin. 2011, A&A, 536, 19
Reynolds, R. J. 1990, in IAU Symp. 139, The Galactic and Extragalactic Background Radiation, ed. S. Bowyer & C. Leinert (Dordrecht: Kluwer), 157
Ryu, K., Min, K.-W., Park, J.-W., et al. 2006, ApJ, 644, 185
Schlegel, D. J., Finkbeiner, D. P., & Davis, M. 1998, ApJ, 500, 525
Sembach, K. R., Savage, B. D., & Jenkins., E. B. 1994, ApJ, 421, 585
Seon, K.-I., & Witt, A. N. 2012, ApJ, 758, 109
Seon, K.-I., Yuk, I.-S., Ryu, K.-S., et al. 2004, JASS, 21, 399
Sharpless, S. 1959, ApJS, 4, 257
Sujatha, N. V., Shalima, P., Murthy, J., et al. 2005, ApJ, 633, 257
Tachihara, K., Abe, R., Onishi, T., et al. 2000, PASJ, 52, 1147
Tetzlaff, N., Neuhäuser, R., & Hohle, M. M. 2010, MNRAS, 410, 190
Thompson, G. I., Nandy, K., Jamar, C., et al. 1978, Catalogue of Stellar Ultraviolet Fluxes. A Compilation of Absolute Stellar Fluxes Measured by the Sky Survey Telescope(S2/68) Aboard the ESROSatellite TD-1 (London: Science Research Council)
Van Buren, D., & McCray, R. 1988, ApJL, 329, L93
van Dishoeck, E. F., & Black, J. H. 1986, ApJS, 62, 109
Villamariz, M. R., & Herrero, A. 2005, A&A, 442, 263
Weingartner, J. C., & Draine, B. T. 2001, ApJ, 548, 296
Wood, K., Haffner, L. M., Reynolds, R. J., et al. 2005, ApJ, 633, 295